AUTOMATIC RETINAL VESSEL DETECTION AND TORTUOSITY MEASUREMENT

Temitope Mapayi[✉,1], Jules R. Tapamo[1], Serestina Viriri[2] and Adedayo O. Adio[3]

[1]School of Engineering, University of KwaZulu-Natal, Durban, 4041, South Africa; [2]School of Mathematics, Statistics, and Computer Science, University of KwaZulu-Natal, Durban, 4041, South Africa; [3]Department of Ophthalmology, University of Port Harcourt, Port Harcourt, Nigeria.
e-mail: mapayit@ukzn.ac.za; tapamoj@ukzn.ac.za; viriris@ukzn.ac.za; drdayoadio@yahoo.com
(Received November 4, 2015; revised May 20, 2016; accepted June 17, 2016)

ABSTRACT

As retinopathies continue to be major causes of visual loss and blindness worldwide, early detection and management of these diseases will help achieve significant reduction of blindness cases. However, an efficient automatic retinal vessel segmentation approach remains a challenge. Since efficient vessel network detection is a very important step needed in ophthalmology for reliable retinal vessel characterization, this paper presents the study on the combination of difference image and *k*-means clustering for the segmentation of retinal vessels. Stationary points in the vessel center-lines are used to model the detection of twists in the vessel segments. The combination of arc-chord ratio with stationary points is used to compute tortuosity index. Experimental results show that the proposed *k*-means combined with difference image achieved a robust segmentation of retinal vessels. A maximum average accuracy of 0.9556 and a maximum average sensitivity of 0.7581 were achieved on DRIVE database while a maximum average accuracy of 0.9509 and a maximum average sensitivity of 0.7666 were achieved on STARE database. When compared with the previously proposed techniques on DRIVE and STARE databases, the proposed technique yields higher mean sensitivity and mean accuracy rates in the same range of very good specificity. In a related development, a non-normalized tortuosity index that combined distance metric and the vessel twist frequency proposed in this paper also achieved a strong correlation of 0.80 with the expert ground truth.

Keywords: clustering, difference image, *k*-means, retinal vessel, segmentation, tortuosity.

INTRODUCTION

Diabetic retinopathy (DR), an eye disease secondary to diabetes, is a major cause of visual loss and blindness worldwide (WHO; 2010). The focus in the evaluation on DR is usually on hard exudates, microaneurysms and vessel morphology. Retinopathy of prematurity (ROP) has also become a major cause of blindness to children in many middle income countries (O'Sullivan *et al.*; 1997; Varughese *et al.*; 2008; Chen *et al.*; 2008; Gergely and Gerinec; 2009; Hakeem *et al.*; 2012; Adio *et al.*; 2014).

In the face of the global prevalence of DR and ROP, the cases of vision loss and blindness tend to increase in the absence of efficient diagnosis and management approaches of the diseases (Rechtman *et al.*; 2007). The families, communities and countries affected by these epidemics are also likely to suffer serious economic setbacks caused by the financial burden, reduced-earnings and reduced-productivity due to visual impairment and blindness (Atlas; 2013). Ophthalmologists, with the help of detected vessel network, focus on retinal vessel feature analysis during the diagnosis of these diseases. Manual detection and analysis of the retinal vessels has however been a very tedious and time consuming task that requires trained and skilled personnel who are often scarce (Sussman *et al.*; 1982; Verma *et al.*; 2002).

Cost-effective interventions to manage diabetes can prevent the economic setbacks arising from complication such as blindness (Klonoff and Schwartz; 2000). Regular retinal examinations for diabetic patients can help in an early detection of DR and significant reduction of the cases of blindness. Automatic segmentation and analysis of the retinal blood vessels are very important for the automatic detection of DR. Given the fact that the screening of large population of patients can be tedious and time consuming since there is a shortage of specialists, automated approach is cost-effective as it has the potential to increase the productivity of the ophthalmologists in such situations (Abràmoff *et al.*; 2010a,b). Mobile-based diagnostic systems can also be used by field workers attending to larger number of people with diabetes in the rural areas where there are no ophthalmologists (Prasanna *et al.*; 2013). This will yield a cost-effective and efficient early management of DR as patients who need further medical care can be referred to ophthalmologists at the early stage rather than advanced stage of the DR.

Automated vessel segmentation has however been a challenging problem due to complexities such as

noise due to nonhomogeneous illumination caused by different reasons such as; curved surface of the retina, the degree of dilation is highly variable across patients, involuntary movements of the patients eye due to the bright flash-light during the acquisition of the retinal fundus images (Joshi and Sivaswamy; 2008; Li *et al.*; 2012). Although existing methods have made great progress in this field, it remains the subject of on-going research as there is need for further improvement in the detection of both large and thin vessels. Supervised vessel segmentation techniques are computationally expensive since training time is required (Condurache and Aach; 2006; Lupascu *et al.*; 2010). Another major drawback of the supervised vessel segmentation techniques is that their performance is highly dependent on the labelled training sample by experts which could sometimes be extremely difficult, expensive or unavailable (Li and Li; 2013). Furthermore, a new set of labelled training sample is often required for retraining to obtain good segmentation performance when detecting vessels on a new set of retinal images (Staal *et al.*; 2004; Marín *et al.*; 2011).

Although several tortuosity measurement techniques (Lotmar *et al.*; 1979; Hart *et al.*; 1997, 1999; Heneghan *et al.*; 2002; Martinez-Perez *et al.*; 2002; Azegrouz *et al.*; 2006; Grisan *et al.*; 2008; Wilson *et al.*; 2008; Bribiesca; 2013; Lisowska *et al.*; 2014) have been proposed, results obtained suggest the need for further improvement. The Arc-chord ratio techniques (Lotmar *et al.*; 1979; Hart *et al.*; 1999; Heneghan *et al.*; 2002; Martinez-Perez *et al.*; 2002; Azegrouz *et al.*; 2006) failed to differentiate varying vessels when they have the same length but different number of vessel twists. Techniques based on inflection points alone are also not robust enough as all the vessels twists are not sufficiently described using them (Bullitt *et al.*; 2003).

This paper presents an investigatory study on the combination of difference image and *k*-means clustering for retinal vessel network segmentation. A study on the characterization of the detected vessels is also presented.

The rest of this paper is organized as follows. Section two describes several works previously done on the detection of retinal vessels and vessel tortuosity. Section three describes the methods and techniques used for the detection and tortuosity measurement of vessels in this paper. Section four explains the experimental setup, results and discussion, while the conclusion is drawn in section five.

Several retinal vessel segmentation and tortuosity measurement techniques have been proposed in the literature. This section gives a detailed review of segmentation and tortuosity measurement of vessels in retinal images.

Different segmentation methods have been previously proposed for the segmentation of retinal vessels (see (Fraz *et al.*; 2012b) for extensive review up until 2012). These techniques can be divided into two major approaches namely unsupervised and supervised methods.

In supervised vessel segmentation methods, different algorithms (Nekovei and Sun; 1995; Sinthanayothin *et al.*; 1999; Niemeijer *et al.*; 2004; Staal *et al.*; 2004; Soares *et al.*; 2006; Ricci and Perfetti; 2007; Osareh and Shadgar; 2009; Lupascu *et al.*; 2010; Marín *et al.*; 2011; You *et al.*; 2011; Fraz *et al.*; 2012c, 2013) are used for learning the set of rules required for the retinal vessel extraction. A set of manually segmented retinal vessels by experts are considered as the reference images. These reference images are used for the training phase of the supervised segmentation techniques. The availability of reliable labelled training samples by experts for the supervised segmentation methods could sometimes be expensive or unavailable.

Fraz *et al.* (2012c, 2013) implemented a supervised segmentation technique based on ensemble classifier of bootstrapped decision trees for the segmentation retinal vessel network. Lupascu *et al.* (2010) implemented a supervised segmentation technique for detecting vessels using Ada-Boost classifier. A feature vector comprising of local and spatial properties of the vessels was generated from the responses of various filters (matched filters, Gabor wavelet transform, Gaussian filter and its derivatives). Ada-Boost classifier was further trained and used to classify each pixel as either vessel or non-vessel. The drawback of this method is the high computational time of 125 seconds required to segment vessels in each retinal image. Another drawback of this method is its inability to detect the thin vessels as retinal vessels width vary from 15 pixels in very large vessels to 3 pixels in small vessels across the fundus images (Li *et al.*; 2012).

Marín *et al.* (2011) generated a 7-D vector composed of gray-level and moment invariants-based features for pixel representation, while a multilayer feed forward artificial neural network (ANN) classifier was used for the vessel segmentation. Nekovei and Sun (1995) used a back-propagation ANN for the segmentation of blood vessels in angiography. ANN was trained using ground truth images of manually labelled angiograms. The ANN was finally applied to segment the blood vessels in the angiograms. Sinthanayothin *et al.* (1999) combined principal component analysis (PCA) with ANN for the localization of anatomical structures in retinal images.

Niemeijer *et al.* (2004) implemented vessel segmentation method based on pixel classification. Each pixel of the green plane of the retinal image and responses of Gaussian matched filter were used to construct feature vectors. Consequently, these feature vectors were classified using a kNN classifier. Osareh and Shadgar (2009) applied multi-scale Gabor filters, and PCA for the extraction of features in the retinal image. The features generated were consequently used to classify the pixels of the retinal images as either vessels or non-vessels using Gaussian mixture model (GMM) and support vector machines (SVM). Ricci and Perfetti (2007) proposed automated vessel segmentation based on line operators. Two segmentation methods were considered. One of the segmentation methods used two orthogonal line detectors with the gray level of the target pixel to construct a feature vector for supervised classification using a support vector machine. Although the technique had a good performance, there are however high false detection around the border of the optic disc. The need for a new set of training samples and the retraining of classifier before applying it on a new dataset also remains the drawback of the method.

Soares *et al.* (2006) implemented the combination of two-dimensional (2-D) Gabor wavelet transform and Bayesian classifier for retinal vessel segmentation. A feature vector comprising a multi-scale 2-D Gabor wavelet transform responses and pixel intensity was generated from the retinal images. Each pixel in the retinal image was further classified as vessel or background tissue using a Bayesian classifier. Although the technique had a good performance, segmentation of thinner vessels as well as false detection around the border of the optic disc remains a challenge. The need for a retraining of classifier before applying it on a new dataset also remains the limitation of this method. Staal *et al.* (2004) utilized ridge information and kNN classifier with sequential forward feature selection for retinal vessel segmentation. One of the drawbacks of the technique in (Staal *et al.*; 2004) is its inability to segment thinner vessels. This method is also expensive as it requires a time consuming manual labelling (about 2 hours per image) and a retraining of the classifier before applying it on a new dataset. The need for a retraining of classifier before applying it on a new dataset also remains the limitation of this method. You *et al.* (2011) combined radial projection with SVM using a semi-supervised self-training approach for the segmentation of vessels. Radial projections were used to locate the vessel centre-lines and the low contrast blood vessels. Having enhanced the vessels using modified steerable wavelet, feature vector was generated using line strength measures. SVM classifier was further used in a semi-supervised self training manner for the classification of each pixel as either vessel or non-vessel. A supervised classification approach utilizing multi-scales vesselness and texture features was proposed by Poletti and Ruggeri (2012) to segment the retinal vessel network in wide-field images acquired with RetCam fundus camera. Poletti and Grisan (2014) proposed a supervised technique based on ADABoost classifier using an array of optimal discriminative convolution kernels for detection of vessels in retinal images.

The approaches based on unsupervised classification, on the other hand, attempt to find inherent patterns of blood vessels in retinal images that can be further used to determine that a particular pixel belongs to vessel or not. The training data or hand labelled ground truths are not needed for the design of algorithm in these approaches. These approaches are matched filter-based (Chaudhuri *et al.*; 1989; Hoover *et al.*; 2000; Chanwimaluang and Fan; 2003; Cinsdikici and Aydın; 2009; Zhang *et al.*; 2010; Chakraborti *et al.*; 2014), scale space-based (Martínez-Pérez *et al.*; 1999; Grisan *et al.*; 2004; Vlachos and Dermatas; 2010; Poletti *et al.*; 2011; Wang *et al.*; 2013), tracking-based (Yin *et al.*; 2013), model-based (Szpak and Tapamo; 2008; Xiao *et al.*; 2013), adaptive thresholding-based (Jiang and Mojon; 2003; Cornforth *et al.*; 2005; Akram and Khan; 2013; Mapayi *et al.*; 2014), mathematical morphology-based (Zana and Klein; 2001; Mendonca and Campilho; 2006; Jiménez *et al.*; 2010; Fraz *et al.*; 2011; Miri and Mahloojifar; 2011; Fraz *et al.*; 2012a) and clustering-based (Tolias and Panas; 1998; Yang *et al.*; 2008; Kande *et al.*; 2010; Lupaşcu and Tegolo; 2011a,b; Sun *et al.*; 2011; Saffarzadeh *et al.*; 2014).

Chaudhuri *et al.* (1989) implemented matched filter response (MFR) by initially approximating the intensity of gray-level profiles of the cross-sections of retinal vessels using a Gaussian shaped curve. An Otsu thresholding technique was further applied to the matched filter response image to segment the retinal vessels. The proposed technique however had a poor detection of the vessels. Hoover *et al.* (2000) segmented retinal vessels by applying a threshold probing technique combining local vessel attributes with region-based attributes on MFR image. While compared to the technique used in (Chaudhuri *et al.*; 1989) where a basic thresholding of an MFR was used, the method proposed in (Hoover *et al.*; 2000) reduced the false positive rate by as much as 15 times. Chanwimaluang and Fan (2003) proposed the combination of matched filter and entropy for the segmentation of retinal vessels. The performance measure of the proposed technique was only visual. Cinsdikici and Aydın (2009) implemented

the combination of matched filter and ANT colony algorithm for the detection of retinal vessels. Zhang *et al.* (2010), having identified that the general matched filter responds to both vessels edges and the non-vessel edges, extended the general matched filter with the first-order derivative of the Gaussian properties of the retinal vessels. The improved technique was, however, faced with the inability to segment the thinner vessels. Chakraborti *et al.* (2014) implemented an unsupervised segmentation technique that combines vesselness filter and matched filter using orientation histogram for the segmentation of retinal vessels.

Martínez-Pérez *et al.* (1999) used a combination of scale space analysis and region growing to segment the vessel network. Vlachos and Dermatas (2010) proposed a retinal vessel segmentation method based on multi-scale line-tracking procedure and morphological post-processing. Wang *et al.* (2013) proposed multi-wavelet kernels and multi-scale hierarchical decomposition. Vessels were enhanced using matched filtering with multi-wavelet kernels. Yin *et al.* (2013) implemented a probabilistic tracking-based method for vessel segmentation. A Bayesian method with maximum a posteriori (MAP) was used for detecting the retinal vessel edge points. Li *et al.* (2006) combined multi-scale analysis based on Gabor filters, scale multiplication, and region based thresholding to achieve adaptive thresholding for vessel segmentation.

Szpak and Tapamo (2008) used gradient based approach and level set technique for the segmentation of retinal vessels. The proposed technique was however unable to detect the thinner vessels. Xiao *et al.* (2013) proposed a Bayesian method with spatial constraint for the segmentation of retinal vessels. The spatial dependence of the posterior probability of each pixel in relation to their neighboring pixels was utilized. An energy function was further defined and a modified level set approach was used for the vessel segmentation.

Jiang and Mojon (2003) implemented an adaptive local thresholding based on a verification-based multi-threshold probing scheme for the detection of vessel network. Vessels' properties such as contrast, curvilinear angle, width, and size were modelled into the verification phase, and a number of thresholds were used to probe and detect vessel network. The combination of the resulting detected vessel networks obtained from probed thresholds followed by post processing techniques was used to generate the final segmented vessel network. The technique was however faced with the limitations of some unconnected vascular structures and the inability to detect the thinner vessels. Akram and Khan (2013) enhanced the vascular pattern using 2-D Gabor wavelet and

followed by a multilayered thresholding technique that applied different threshold values iteratively to generate gray level segmented image. Cornforth *et al.* (2005) applied wavelet analysis, supervised classifier probabilities and adaptive threshold procedures, as well as morphology-based techniques. A comparative study of global thresholding techniques previously implemented by Mapayi *et al.* (2015) showed that global thresholding approaches are limited at efficiently segmenting thin retinal vessels. In another study, Mapayi *et al.* (2014) implemented an adaptive thresholding technique utilizing different types of local homogeneity information for retinal vessel segmentation.

Zana and Klein (2001) implemented a vessel segmentation method based on the use of mathematical morphology and cross-curvature evaluation. Mendonca and Campilho (2006) combined differential filters for center-line extraction with morphological operators for filling vessel segments considering intensity and morphological properties. Miri and Mahloojifar (2011) found ridges by applying multi-structure elements to enhanced retinal image. Morphological operators by reconstruction was further applied to get rid of the ridges outside the vessel tree. Fraz *et al.* (2011, 2012a) combined vessel centre-lines detection and morphological bit plane slicing for the detection of vessel network in retinal images. Jiménez *et al.* (2010) implemented vessel centre-lines detection and a combination of morphological operations for retinal vessel segmentation.

Kande *et al.* (2010) combined matched filtering and a spatially weighted fuzzy C-means for vessel segmentation in retinal images. Lupaşcu and Tegolo (2011a,b) having trained a self-organizing map (SOM) on retinal images, proposed two clustering techniques for vessel segmentation. The map was divided into two classes using *k*-means clustering technique (Lupaşcu and Tegolo; 2011a) and modified Fuzzy C-Means clustering algorithm (Lupaşcu and Tegolo; 2011b). A post-processing technique based on hill climbing strategy on connected components was further applied to detect the vessel network (Lupaşcu and Tegolo; 2011a,b). Saffarzadeh *et al.* (2014) implemented a preprocessing phase based on *k*-means followed by the use of multi-scale line operators for the detection of retinal vessel network. With the use of *k*-means, the visibility of the vessels was enhanced and the impact of bright lesions reduced. The retinal vessels were finally detected using the line detection operator in three scales. Sun *et al.* (2011) implemented morphological multi-scale enhancement in combination with fuzzy filter and watershed transformation for vascular segmentation. Tolias and Panas (1998) implemented a fuzzy C-means algorithm to segment vessels in

retinal angiogram images. The technique however did not segment thinner vessels due to their low contrast against background. An automatic extraction of the vascular structure in retinal images using a sparse tracking technique was also proposed in Grisan *et al.* (2004). Poletti *et al.* (2011) proposed an automatic extraction of vessel centerline in wide-field ROP retinal images using a sparse tracking scheme. An hybrid approach comprising of a fuzzy clustering and mathematical morphology was proposed by Yang *et al.* (2008). A morphological top-hat operation was used for retinal image smoothing and background information removal. The vessels were then extracted through fuzzy clustering.

Retinal vessel tortuosity is one of the early symptoms of some retinopathies (Wasan *et al.*; 1995) and are of great importance in the diagnosis of ROP (Davitt and Wallace; 2009). Retinal vessel network tortuosity is the measure of twists and curvature of a vessel. Retinal vessel tortuosity measures are used to determine the state of retinal images as either healthy or diseased even when there are no visible pathologies as shown in Fig. 1. One of the first changes in vessels morphology to occur in DR patients is the increase in vessel tortuosity (Scheie; 1953; Kristinsson *et al.*; 1997; Owen *et al.*; 2008; Taarnhøj *et al.*; 2008; Dougherty *et al.*; 2010; Onkaew *et al.*; 2011; Chakravarty and Sivaswamy; 2013).
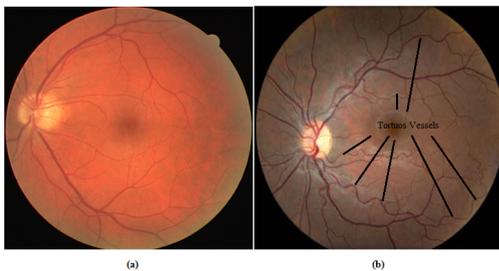
Fig. 1: (a) Coloured retinal image with normal vessels (b) Coloured retinal image with tortuous vessels.

Tortuosity has been shown to be a more reliable vascular parameter in differentiating ROP severity than vessel width (Capowski *et al.*; 1995). High blood pressure has been linked to diabetes due to its relationship with hypertension (Bedell; 1945; Kylstra *et al.*; 1986; Patasius *et al.*; 2007) and tortuosity has also been identified as an indicator of high blood pressure. Degeneration of retinal vessel walls and changes in their elastic properties have been identified to be major causes of vessel tortuosity (Azegrouz *et al.*; 2006). The duration of diabetic disease has a strong effect on changes in vessel tortuosity (Lim *et al.*; 2010; Sasongko *et al.*; 2010).

Although vessel tortuosity are visually analyzed and determined by ophthalmologists based on the curvature and twisting rate of vessels, qualitative grading of vessel tortuosity suffers from inter-observer and intra-observer variations (Wolffsohn *et al.*; 2001). Several methods have been applied to quantitatively determine the measure of tortuosity of a vessel (Bullitt *et al.*; 2003). The term often called the tortuosity index (TI), is used for the estimation of the vessel tortuosity. TI provides a reproducible measure of vessel characteristics.

Vessel tortuosity was computed as the ratio of the actual vessel length to the length of the underlying chord (Lotmar *et al.*; 1979; Hart *et al.*; 1999; Heneghan *et al.*; 2002; Martinez-Perez *et al.*; 2002; Wilson *et al.*; 2008). This technique assumes a vessel to be non-tortuous if it is straight line and tortuous while the radius of curvature is longer than the chord length of the vessel. The techniques however failed to differentiate varying vessels with the same length but with different tortuosity.

Hart *et al.* (1997) implemented automatic tortuosity measurement using integral curvature methods. Dougherty and Varro (2000) used second derivatives along central axis of the blood vessels for automatic tortuosity measurement. Bullitt *et al.* (2003) applied the number of inflection points for the automatic vessel tortuosity measure. Grisan *et al.* (2003, 2008) implemented automatic tortuosity measures using arc to chord ratio and the points of changing curvature sign. The vessel extraction and inflection point placement was however done manually (Sinthanayothin *et al.*; 2010; Onkaew *et al.*; 2011). Capowski *et al.* (1995) addressed tortuosity measurement using the number of direction changes in vessel course. Azegrouz *et al.* (2006) proposed a vessel-thickness tortuosity measurement method utilizing the average of the two curvature values computed at two boundary points of the vessel.

Generally, automatic tortuosity measurement methods based on local tortuosity measurement performs better while compared to the techniques based on global tortuosities (Wilson *et al.*; 2008). However, the contribution of each local tortuosity measure is considered for computing the global tortuosity measure.

Although, much has been achieved in the previous works, the performances obtained from literature suggest the need for further work to address the robust segmentation of large and thinner retinal vessels. There is also need to investigate an efficient approach for vessel tortuosity measurement.

MATERIALS AND METHODS

Since efficient vessel network detection is a very important step needed in ophthalmology for reliable retinal vessel characterization, a robust segmentation technique that performs the detection of large and thin vessels in a timely manner is highly needed. This section presents an unsupervised vessel segmentation approach to address the problems of inability to detect the thinner vessels (Martínez-Pérez *et al.*; 1999; Vlachos and Dermatas; 2010; Saffarzadeh *et al.*; 2014; Mapayi *et al.*; 2015) connectivity loss in vessel network (Jiang and Mojon; 2003). Since unsupervised vessel segmentation methods are not dependent on labelled training set, the method investigated in this paper also overcomes the major drawback of supervised segmentation methods which is their high dependence on the labelled training (Li and Li; 2013) with the retraining of the classifiers (Soares *et al.*; 2006; Marín *et al.*; 2011). The detailed description of the materials with the vessel segmentation methods and tortuosity measurement techniques investigated in this paper are further presented in sections Materials, Vessel Segmentation and Vessel Tortousity Measurement respectively.

MATERIALS

Experiments were carried out using MATLAB 2010a on an Intel Core i5 2410M CPU, 2.30 GHz, 4GB of RAM. The proposed method was evaluated using the retinal images on the publicly available databases (DRIVE; 2004; STARE; 2000). DRIVE (2004) is a publicly available database consisting of 40 colour retinal fundus images. These images were obtained from a diabetic retinopathy screening program in the Netherlands. The images were acquired using a Canon CR5 non-mydriatic 3CCD camera with a 45 degree field of view (FOV). Each image was captured using a 24-bit RGB colour at 768×584 pixels. The FOV of each image is circular with a diameter of approximately 540 pixels. This set of forty colour retinal fundus images are divided into two groups. The first group of the images is made up of twenty images which are a training set for supervised segmentation techniques. The training set are, however, not used in this paper because we applied an unsupervised segmentation method. The second group is a testing set made up of twenty images. All the human observers that manually segmented the vessels in the retinal images were instructed and trained by an experienced ophthalmologist. A set of manual segmentations of the vessel network is available for the training images. Two manual segmentations sets X and Y are available for the test cases. In set X, 577,649 pixels were marked as vessel and 3,960,494 pixels as background (12.7% vessel). In set Y, 556,532 pixels were marked as vessel

and 3,981,611 as background (12.3% vessel). It was, however, observed that it took a human observer an average time of 7200 seconds (2 hours) to segment the vessels in each of the retinal images. Set X of the manual segmentations of the test cases is used as gold standard (ground truth), while set Y is often compared to the performance of the automatic segmentation techniques on the database. STARE (STructured Analysis of the Retina) STARE (2000) is a publicly available database that consists of 20 retinal images captured with the use of TopCon TRV-50 fundus camera with 24-bit grey-scale resolution and spatial resolution of 700×605 pixels. The approximate diameter of the FOV is 650 pixels. Two observers manually segmented all the images. The first observer segmented 10.4% of pixels as vessel, against 14.9% vessels for the second observer. The segmentations of the two observers are fairly different in that the second observer segmented many more of the thinner vessels than the first one. The 20 manually segmented images provided by the first observer is used as the ground truth for the comparative performance evaluation of different vessel segmentation algorithms in the literature.

It is however important to note that one of the major reason why the first and second observer disagreed in the manual segmentations of the retinal vessels was because of the difficulty to distinguish vessel pixels due to JPEG-artefacts. The decisions of the human observers at distinguishing pixels at vessel borders as either vessel or non-vessel are also subjective. Although the second observer labelled more pixels as vessels when compared to the first observer on the STARE database, the first observer took a more conservative view of the boundaries of vessels and in the identification of small vessels when compared to the second observer. Hence, the manual segmentation of the first observers of DRIVE and STARE databases are used as the ground truth for the comparative performance evaluation of different vessel segmentation algorithms in the literature.

In a related development, 50 digital fundus images containing 50 different vessel segments used for the vessel tortuosity measurement. Expert's ground truth that determined the state of each vessel segment as either tortuous or normal was also obtained from a consultant ophthalmologist.

VESSEL SEGMENTATION

The green component of the coloured retinal image is used for segmentation since it provides the best vessel-background contrast (Staal *et al.*; 2004). A detailed description of the vessel segmentation approach investigated in this paper is given as:

1. Extraction of the green channel of the coloured fundus image.

2. Process the green channel of the retinal image using different filtering techniques.

3. Generate the difference image.

4. Segment the retinal vessels from the generated difference image using *k*-means clustering.

5. Implement a post-processing phase that combines median filter and morphological opening for the removal of misclassification.

Filtering Techniques

The green channel of the retinal image is enhanced using different filtering techniques. Linear filters such as mean filter and Gaussian filter are used for smoothing images. Although these filters reduce image noise, they are however weak at preserving edges in an image. Non-linear filter, particularly median filter, is efficient at removing image noise as well as preserving edge information in images. It is however worth noting that the selected filter window sizes should not be too large in order to efficiently manage the noise due to illumination variation conditions of the retinal image. It is also important to carefully select window sizes that have sufficient data points for good enhancement. The window sizes of the filters applied in this work are empirically selected. For the purpose of investigation in this paper, mean and Gaussian filters are considered for the convolution while median filter is used for the filtering of the retinal image. The image padding does not affect the retinal image as there are black background pixels after the circular field of view. We replicated the border pixel values (which are zeros) for the image padding at the border of the retinal image (i.e including the background), and this has no effect as the background pixels around the border are also black.

Difference Image

A difference image is generated by subtracting the green channel of the coloured retinal image from the convolved of filtered retinal image to balance the illumination of the retinal image. The difference image $D(x,y)$ is given below as:

$$D(x,y) = U(x,y) - V(x,y) , \qquad (1)$$

where U is the convolved or filtered retinal image, V is the green channel of the retinal image. $D(x,y) = \{D_\rho(x,y), D_\upsilon(x,y), D_\sigma(x,y)\}$, where $D_\rho(x,y)$ is the difference image based on median filter (DIMDF), $D_\upsilon(x,y)$ is the difference image based on mean filter (DIMNF) and $D_\sigma(x,y)$ is the difference image based on Gaussian filter (DIGF). A model that combines two

possible difference images was also investigated. The combinations obtained are:

$$D_\upsilon^\rho = D_\rho(x,y) + D_\upsilon(x,y) , \qquad (2)$$
$$D_\sigma^\upsilon = D_\upsilon(x,y) + D_\sigma(x,y) , \qquad (3)$$
$$D_\sigma^\rho = D_\rho(x,y) + D_\sigma(x,y) , \qquad (4)$$

where D_υ^ρ is the combination of median filter and mean filter based difference images (DIMDMNF), D_σ^υ is the combination of mean filter and Gaussian filter based difference images (DIMNGF) and D_σ^ρ is the combination of median filter and Gaussian filter based difference images (DIMDGF). The results obtained in Eqs. 2–4 are normalized to the interval [0, 255]. Fig. 2 shows the coloured retinal image, the green channel of the coloured retinal image and the difference image obtained using the DIMDF investigated in this paper.
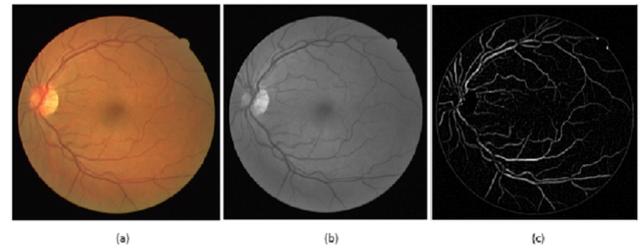
Fig. 2: Coloured retinal image on DRIVE database (a), green channel of the coloured retinal image (b), difference image based on DIMDF (c).

K-Means Clustering

K-means clustering is an unsupervised segmentation technique used in defining the natural group of pixels in an image. This is achieved by classifying input image data points into different classes through a set of distances computed using the image data points and centroids. *K*-means clustering technique is used for dividing n sample input data points of $X = \{x_1, x_2, ..., x_n\}$ into a group of *k* clusters. This is achieved by considering the similarities among the input points within the same cluster as well as the differences among the different clusters. Sum of squared errors is a very useful criterion measure for clustering. Given *k* clusters, the sum of squared errors is computed as:

$$\text{SSE} = \sum_{i=1}^{k} \sum_{x_j \in S_i} ||x_j - \mu_i||^2 , \qquad (5)$$

such that μ_i is the centroid of the ith cluster S_i, $\{i = 1, 2 \dots k.\}$.
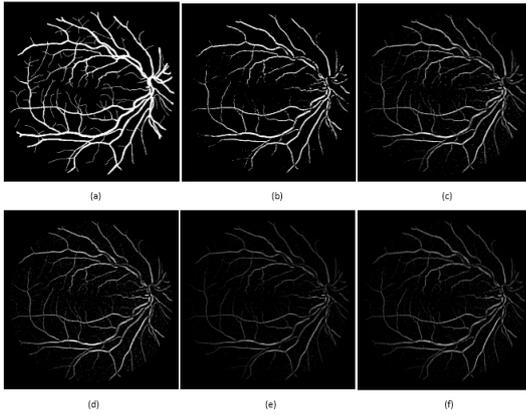
Fig. 3: Segmentation results of different values of K before post-processing(a) Gold standard image on DRIVE database (b) K=2 (c) K=4 (d) K=6 (e) K=8 (f) K=10.

The *k*-means clustering technique is used to segment the vessel network from the background tissue in the retinal images using the results generated from Eqs. 1–4. This clustering technique was applied on the retinal image pixel intensities. In order to determine the number of clusters *k*, a range of values were investigated. Fig. 3 shows the impact of different values of k for the detection of the vessel network. Randomly, five different values of *k*, $k = 2$, $k = 4$, $k = 6$, $k = 8$, and $k = 10$ are shown in Fig. 3. It will be observed that when $k = 2$, the smaller vessels were not detected. There was however an improvement in the detection of the vessels when $k = 4$. The were better detection of vessels when $k = 6$, $k = 8$ and $k = 10$. The value $k = 10$ was applied for the *k*-means clustering technique applied in this paper. Fig. 4 shows the detected vessels after applying *k*-means clustering on the difference images.

POST-PROCESSING

Median filter and morphological opening are used for the post-processing phase to remove noisy pixels appearing to be broken vessels and restore the connectivity of the background tissues (black background) while the several vessel networks are still preserved. Median filtering is a non-linear smoothing operation often used in image processing to reduce noise and preserve edges at the same time. In this research, the median filtering is performed by moving a 2×2 sliding-window through all the pixels of the binarized retinal image containing detected vessels. When the chosen mask is greater than 2×2, the median filter categorizes some of the smaller retinal vessels as noise. This is followed by morphological opening. In the application of morphological opening to the filtered image, erosion is applied to remove the remaining noisy pixels and

dilation is subsequently applied. The morphological opening with line structuring elements orientated in five different directions namely 0°, 30°, 60°, 120°, 150° was applied. Another mophological operator applied is the area opening. This technique removes the remaining noisy pixels appearing to be broken vessels using the connectivity value 8. After this, the FOV mask is subtracted from the segmented image to obtain the detected vessel in the circular field of view. Given that the filtered segmented image is S_{im}^{filtered}, the final output image after the application of morphological opening is computed as:

$$\gamma(S_{im}^{\text{filtered}}) = \delta(\varepsilon(S_{im}^{\text{filtered}})) , \qquad (6)$$

where $\gamma(S_{im}^{\text{filtered}})$ is the final segmented vessel network after post-processing and $\varepsilon(S_{im})$ describes the application of erosion and $\delta(S_{im}^{\text{filtered}})$, the application of dilation.
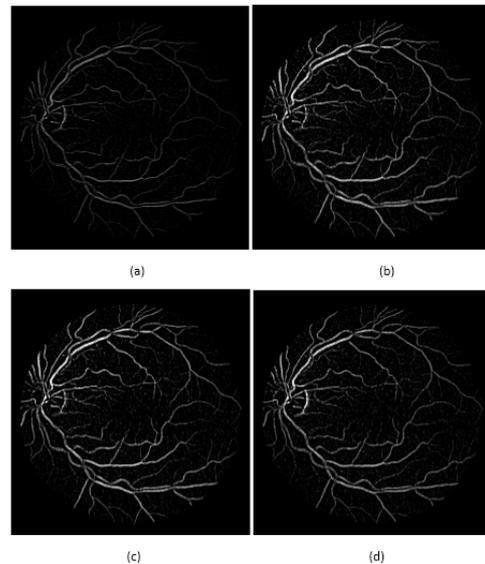
Fig. 4: Detected vessels based on *k*-means and difference image before post-processing(a) *k*-means and DIMDF (b) *k*-means and DIMDGF (c) *k*-means and DIMDMNF (d) *k*-means and DIMNGF.

VESSEL TORTOUSITY MEASUREMENT

Retinal vessel network tortuosity is the measure of twists and curvature of a vessel (Grisan *et al.*; 2003, 2008; Onkaew *et al.*; 2011; Chakravarty and Sivaswamy; 2013). Several clinical studies have described the relation between vessel tortuosity and retinopathies such as DR, ROP (Scheie; 1953; Capowski *et al.*; 1995). Fig. 5 shows the variation in the directional changes, frequency of twists and the differences in the vessel lengths of the different vessels a, b, c, d, e, f and g.

Description of Tortuosity

With the help of ophthalmologic rules and clinical definition, the metric that provides numeric index for vessel tortuosity measurement is utilized (Bullitt *et al.*; 2003). Rather than inflection points alone (Bullitt *et al.*; 2003), the stationary points of the vessel are considered to be very important for computing the tortuosity measure in this paper. A combination of arc-chord ratio with stationary points are used to compute tortuosity index using the local tortuosity measurement approach. Fig. 6 shows a sample vessel of interest is marked, detected vessel of interest and skeletonized form of detected vessel of interest.

The tortuosity measure applied in this paper utilizes the chord length, arc length and the frequency of vessel curve using the stationary points as described in Algorithm 1. The blood vessel is skeletonised to extract the center line of the vessel.

The chord length L_{chord} of the skeletonised blood vessel is defined as

$$L_{chord} = \sqrt{(x_n - x_1)^2 + (y_n - y_1)^2} \,, \qquad (7)$$

where L_{chord} is the length of the straightline connecting the two end-points of the skeletonised blood vessel.

The arc length L_{arc} of the skeletonised blood vessel is defined as

$$L_{arc} = \sum_{i=1}^{n-1} \sqrt{(x_{i+1} - x_i)^2 + (y_{i+1} - y_i)^2} \,, \qquad (8)$$

where L_{arc} is the actual length of the skeletonised blood vessel.

The pixel locations of skeletonised blood vessels are extracted to plot a vessel description graph as shown in Fig. 7. A set of frequent smaller swings occurred on the skeletonised vessel segment as a result of noise. In order to efficiently detect the number the stationary points, a moving average filter with span n = 5 was applied to smoothen the smaller swings that occurred on the skeletonised vessels to remove the noise. The stationary points of the vessel description graph are computed using the gradients of the vessel description graph. We applied a 1-point difference scheme. With such scheme, each gradient is computed as either 0, 1 or -1. With the help of the 1-point difference, a change of direction in the vessels can also be detected. The stationary points are points on the vessel description graph where the gradient is zero. There are however three major types of stationary points: minimums, maximums and inflection points as illustrated in Fig. 8 and Fig. 9 (Thomas; 1996).
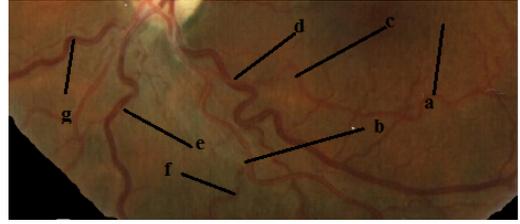
Fig. 5: Retinal vessels with different twists.
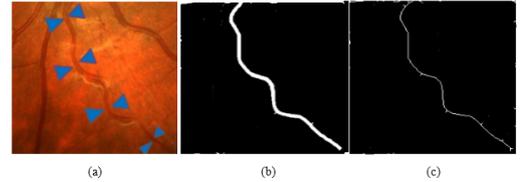
Fig. 6: Coloured retinal with vessel of interest marked (a), detected vessel of interest (b), and skeletonization of detected vessel of interest (c).
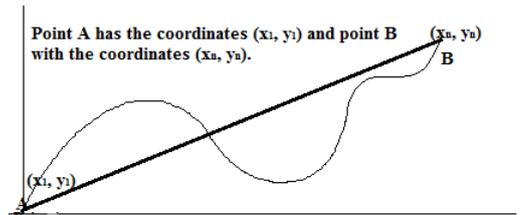
Fig. 7: Vessel graph describing X and Y coordinates of skeletonised blood vessels.
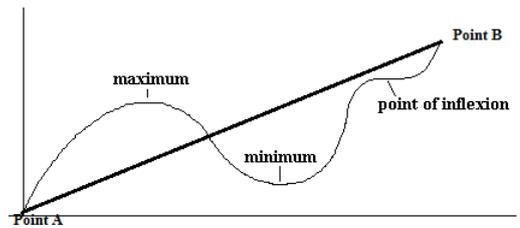
Fig. 8: Graph describing different stationary points between point A & point B.

Given the skeletonised blood vessel T with vessel coordinates X and Y, the gradients of the vessel description graph are computed as:

$$G = \frac{dY}{dX} \,, \qquad (9)$$

such that $X = \{x_1, x_2, \ldots, x_n\}$, $Y = \{y_1, y_2, \ldots, y_n\}$, $G = \{g_1, g_2, \ldots, g_n\}$ and $-1 \leq G \leq 1$ where $G\varepsilon\mathbb{I}$.

The nature of each type of the stationary points is shown in Fig. 9 and Table 1:

Algorithm 1: Vessel Twist Detection Based on Stationary Points Algorithm

---

Input: S1, S2, S3, S4 are the sets of stationary point detectors. T is the thinned segmented vessel.

Output: SPC_{count} is total number of vessel twists, D_i is the set of gradient pattern obtained from the detectors and E_j is the set of gradient pattern obtained from the thinned segmented vessel

```
/* Computes and Updates the computed gradient patterns of the detectors
   based on stationary points.                                          */
```
1 **for** $i \leq 4$ **do**
2   **while** $s \in S_i$ **do**
```
       /* diff computes gradients.                                      */
```
3       $D_i = diff(s)$ $UpdateDetectorPattern(D_i)$
4   **end**
5 **end**
```
   /* Initialize the vessel twist counter to zero.                      */
```
6 $counter \leftarrow 0$
```
   /* Updates the computed gradient patterns of the segmented vessel.   */
```
7 **while** $t \in T$ **do**
8    $E_j = diff(t)$
9    $UpdateRealVesselPattern(E_j)$ **for** $i \leq 4$ **do**
10   **if** *Matches* (E_j, D_i) **then**
```
          /* Increments the vessel twist counter.                       */
```
11          $counter++$
12   **end**
13   **end**
14 **end**
15 $SPC_{count} \leftarrow counter$
16 **return** SPC_{count}
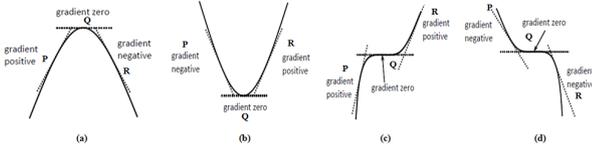
Fig. 9: Maximal point (a), minimal point (b), points of inflection (c, d).

Table 1: Stationary points nature table.

Sign of $\frac{dy}{dx}$ at P	Sign of $\frac{dy}{dx}$ at R	Graphical Behavior	Inference
+	-	Fig. 9(a)	A turning point corresponding to maximum (S1)
-	+	Fig. 9(b)	A turning point corresponding to minimum (S2)
+	+	Fig. 9(c)	An inflection point (S3)
-	-	Fig. 9(d)	An inflection point (S4)

The stationary points in the vessel description graph are computed using the vector of gradient obtained from Eq. (9) and the nature table in Table 1. In Algorithm 1, the gradient patterns D_i of the stationary points detectors S1, S2, S3, S4 are computed. The vessel twist counter is initialize to zero and updated using UpdateRealVesselPattern as the presence of twists are detected in the vessel by matching the detector patterns D_i with vessel pattern E_j obtained from the thinned segmented vessel. The total number of twists, SPC_{count}, is then computed. We investigate a normalized TI metric TI_{freq1} that combines distance metric and the vessel twist frequency obtained using the stationary points. This is computed as:

$$TI_{freq1} = \frac{SPC_{count}}{L_{chord}}\left((L_{arc} - L_{chord})/L_{chord}\right), \quad (10)$$

where SPC_{count} is the twist frequency of the vessel curves.

Several literature have applied a distance metric by dividing the arc length by the chord length (see Kalitzeos *et al.*; 2013). While the previously presented distance metric divided the arc length by the chord length (Kalitzeos *et al.*; 2013), a different distance

metric that divides the chord length and the number of stationary points by the arc length is used for the non-normalized TI in this study. The non-normalized TI is computed as

$$TI_{freq2} = SPC_{count}(L_{chord}/L_{arc}) . \quad (11)$$

RESULTS

Empirically, we established that using window sizes 11×11, for mean and Gaussian filters, 15×15 for median filter were effective for the detection of the vessel network. The average time taken to segment the vessel networks in each of the retinal image on DRIVE and STARE databases ranges from 3.4 to 4.0 seconds.

The performance measures used are sensitivity, specificity and accuracy. The measures are described in the Eqs. 12–14 below as:

$$Sensitivity = \frac{TP}{TP + FN} , \quad (12)$$

$$Specificity = \frac{TN}{TN + FP} , \quad (13)$$

$$Accuracy = \frac{TP + TN}{TP + TN + FP + FN} , \quad (14)$$

where TP is True Positive, TN is True Negative, FP is False Positive and FN is False Negative.
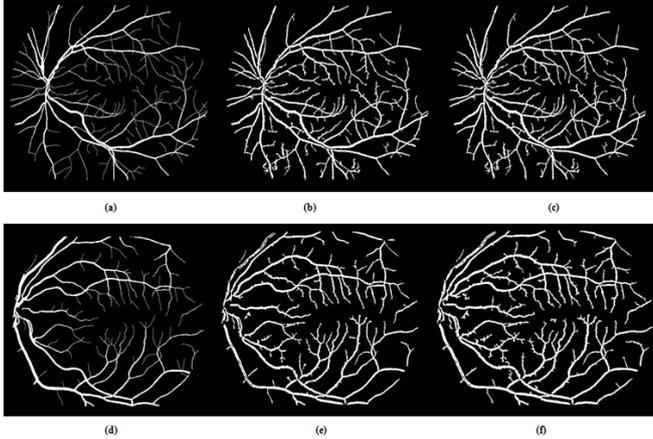
Fig. 10: (a) & (d) STARE database ground truth. (b) & (e) Segmented vessels using k-means with DIMDF. (c) & (f) Segmented vessels using k-means with DIMDMNF.

An event is said to be TP when a pixel is rightly segmented as a vessel and TN when rightly segmented as background. Conversely, an event is said to be FN if a vessel-pixel is segmented to be a background, and a FP when a background pixel is segmented as a pixel in the vessel. Sensitivity measure indicates the ability of a segmentation technique to detect the pixels belonging to vessel while specificity measure indicates the ability of a segmentation technique to detect background pixels. Therefore, the higher the sensitivity rate, the higher the rate of vessel detection. The accuracy measure indicates the degree of conformity of the segmented retinal image to the ground truth.

Table 2: Performance of different segmentation methods on DRIVE database.

Method	Avg. Acc.	Avg. Sens.	Avg. Spec.
Human observer	0.9473	0.7761	0.9725
Chaudhuri *et al.* (1989)	0.8773	0.3357	0.9794
Martínez-Pérez *et al.* (1999)	0.9181	0.6389	0.9496
Zana and Klein (2001)	0.9377	0.6971	0.9769
Jiang and Mojon (2003)	0.9212	0.6399	0.9625
Niemeijer *et al.* (2004)	0.9416	0.7145	0.9801
Staal *et al.* (2004)	0.9442	0.7345	0.9773
Mendonca and Campilho (2006)	0.9463	0.7315	N/A
Soares *et al.* (2006)	0.9466	N/A	N/A
Ricci and Perfetti (2007)	0.9595	N/A	N/A
Szpak and Tapamo (2008)	0.9299	N/A	N/A
Vlachos and Dermatas (2010)	0.9285	0.7468	0.9551
Lupaşcu and Tegolo (2011a)	0.9459	0.6562	N/A
Lupaşcu and Tegolo (2011b)	0.9482	0.6565	N/A
Marín *et al.* (2011)	0.9452	N/A	N/A
Akram and Khan (2013)	0.9469	N/A	N/A
Wang *et al.* (2013)	0.9461	N/A	N/A
Xiao *et al.* (2013)	0.9529	0.7513	0.9792
Yin *et al.* (2013)	0.9267	0.6522	0.9710
Saffarzadeh *et al.* (2014)	0.9387	N/A	N/A
k-Means With DIMDF	**0.9556**	**0.7399**	**0.9766**
k-Means With DIMDMNF	**0.9516**	**0.7581**	**0.9703**
k-Means With DIMNGF	**0.9523**	**0.7079**	**0.9759**
k-Means With DIMDGF	**0.9531**	**0.7518**	**0.9726**

A receiver operating characteristic (ROC) curve performance measure is a plot of the rightly classified pixels, referred to as true positive rate (TPR) versus the fraction of the wrongly classified pixels as vessels, referred to as false positive rate (FPR). Area under the curve (AUC) is a performance measure computed from the ROC curve. The ROC are determined by setting the threshold on the posterior probability. The image with $k = 10$ in Fig. 3 serve as the posterior probabilities.

The differences between the various results achieved by the best methods investigated in this paper are assessed by means of z-test statistics (Foody; 2009). The sensitivity is the proportion of the rightly detected vessel pixel while the accuracy rate is the proportion of the rightly detected pixel in the retinal image. To evaluate the variability of the performance of the different methods on the same dataset, we used the same set of data point samples. The significant difference in average sensitivity rate

indicates the significant difference in the detection rate of the vessels and the significant difference in accuracy rate indicates the significant difference in the accuracy rate of the retinal vessel segmentation. Both measures are very important as good vessel segmentation method for efficient vessel analysis in ophthalmology requires that sensitivity and accuracy rates of the segmentation be good (Mapayi *et al.*; 2015). The statistical significance of a difference between two proportions is evaluated as

$$z = \frac{\mid p_1 - p_0 \mid}{\sqrt{\bar{p}(1 - \bar{p}(\frac{1}{n_1} + \frac{1}{n_0}))}} \, , \qquad (15)$$

where $\bar{p} = (x_1 + x_0)/(n_1 + n_0)$ with x_0 and x_1 representing the number of cases of the rightly detected pixel in the classifications of sample data-points of size n_0 and n_1 respectively. The statistically difference is computed at an asymptotic confidence level of 95% ($\alpha = 0.05$).

K-means with DIMDF has the best average accuracy and average sensitivity rates on DRIVE and STARE databases. DIMDF combined with *k*-means clustering detected majority of large and thin vessels, while very few thinner vessels remain undetected. In a related development, DIMDMNF and DIMDGF while combined with *k*-means yielded higher average sensitivity rates but lesser average accuracy rates while compared to DIMDF combined with *k*-means clustering technique. The increase in sensitivity is as a result of the integration of the other difference image with DIMDF. DIMDF however has the highest average accuracy rate while compared to DIMDMNF and DIMDGF while combined with *k*-means clustering technique. Fig. 11 gives a visual description that compares the results obtained from vessels segmented using DIMDF DIMDMNF and DIMDGF while combined with *k*-means clustering technique on DRIVE database. Fig. 10 and Fig. 12 show the visual results obtained from vessels segmented using DIMDF DIMDMNF, DIMNGF and DIMDGF while combined with *k*-means clustering technique in comparison with the ground truth and the result obtained by Hoover *et al.* (2000) on STARE database. As shown in Figs. 10, 11 and 12, majority of large and thin vessels are detected, a very few thinner vessels still remain undetected. The false detection around the border of the optic disc are higher on the results obtained by using DIMDMNF and DIMDGF while combined with *k*-means clustering but lesser on the results obtained while using *k*-means combined with DIMDF as shown Fig. 11. This is also responsible for the higher average accuracy rate achieved by DIMDF while combined with *k*-means clustering technique. The result obtained while DIMNGF is combined with *k*-means clustering

technique in Fig. 12 however shows that the thinner vessels are not detected.

The performance measures of the different previously proposed techniques on DRIVE and STARE databases are also compared to the proposed techniques in Tables 2 and 3. The average accuracy rate is written by Avg. Acc., average sensitivity rate as Avg. Sens. and average specificity rate as Avg. Spec.
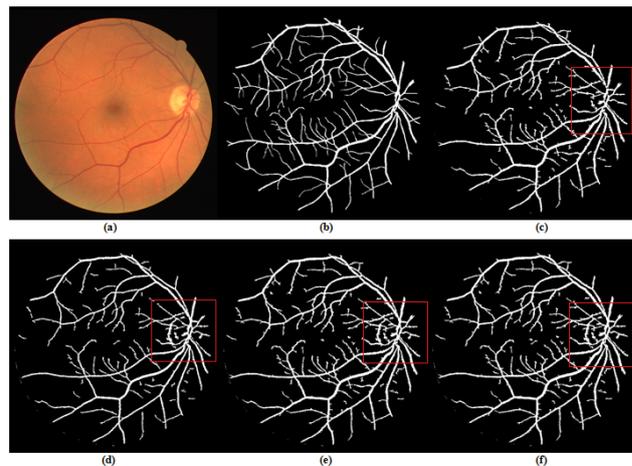
Fig. 11: The red rectangular box indicates the noise rate around the border of the optic disc (a) DRIVE database coloured fundus image (b) DRIVE database gold standard (c) Segmented vessels using *k*-means with DIMDF (d) Segmented vessels using *k*-means with DIMNGF (e) Segmented vessels using *k*-means with DIMDGF (f) Segmented vessels using *k*-means with DIMDMNF.
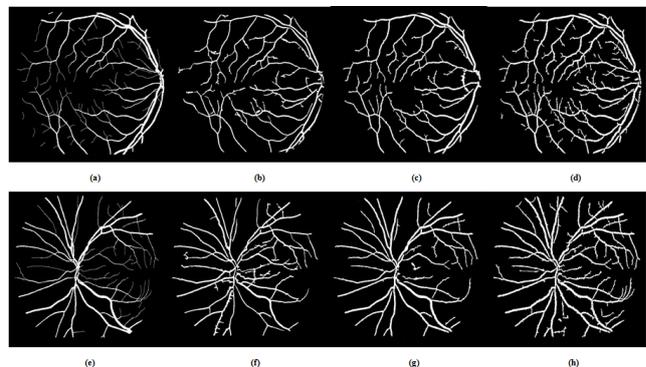
Fig. 12: (a) & (e) STARE database ground truth. (b) & (f) Segmented vessels presented by Hoover (Hoover *et al.*; 2000). (c) & (g) Segmented vessels using *k*-means with DIMNGF (d) & (h) Segmented vessels using *k*-means with DIMDGF.
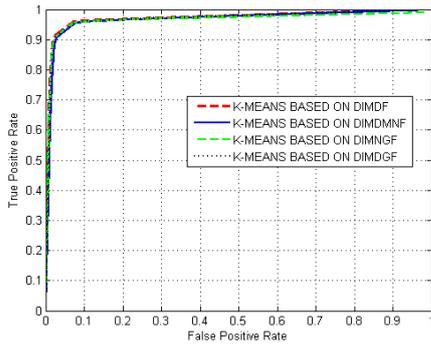
Fig. 13: ROC curves showing the performance of the various difference images combined with *k*-means clustering on DRIVE.
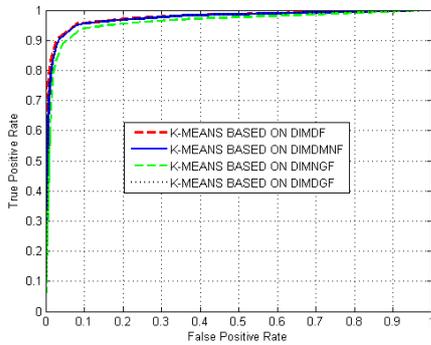
Fig. 14: ROC curves showing the performance of the various difference images combined with *k*-means clustering on STARE.

Table 3: Performance of different segmentation methods on STARE database.

Method	Avg. Acc.	Avg. Sens.	Avg. Spec.
Human observer	0.9354	0.8949	N/A
Hoover *et al.* (2000)	0.9275	0.6751	0.9567
Jiang and Mojon (2003)	0.9009	N/A	N/A
Staal *et al.* (2004)	0.9516	0.6970	N/A
Mendonca and Campilho (2006)	0.9479	0.7123	N/A
Soares *et al.* (2006)	0.9480	N/A	N/A
Ricci and Perfetti (2007)	0.9584	N/A	N/A
Marín *et al.* (2011)	0.9526	N/A	N/A
Akram and Khan (2013)	0.9502	N/A	N/A
Wang *et al.* (2013)	0.9521	N/A	N/A
Xiao *et al.* (2013)	0.9476	0.7147	0.9735
Yin *et al.* (2013)	0.9412	0.7248	0.9666
Saffarzadeh *et al.* (2014)	0.9483	N/A	N/A
***k*-Means With DIMDF**	**0.9509**	**0.7372**	**0.9681**
***k*-Means With DIMDMNF**	**0.9492**	**0.7752**	**0.9633**
***k*-Means With DIMNGF**	**0.9340**	**0.6979**	**0.9526**
***k*-Means With DIMDGF**	**0.9500**	**0.7666**	**0.9648**

Table 4: Comparison of AUC of the proposed techniques with previous works on DRIVE and STARE databases.

Method	AUC DRIVE	AUC STARE
Chaudhuri *et al.* (1989)	0.7878	N/A
Zana and Klein (2001)	0.8984	N/A
Jiang and Mojon (2003)	0.9114	0.929
Niemeijer *et al.* (2004)	0.9294	N/A
Staal *et al.* (2004)	0.9520	0.9614
Soares *et al.* (2006)	0.9614	0.9671
Ricci and Perfetti (2007)	0.9558	0.9602
Marín *et al.* (2011)	0.9588	0.9769
Akram and Khan (2013)	0.963	0.970
Wang *et al.* (2013)	0.9543	0.9682
Saffarzadeh *et al.* (2014)	0.9303	0.9431
***k*-Means With DIMDF**	**0.9735**	**0.9756**
***k*-Means With DIMDMNF**	**0.9749**	**0.9728**
***k*-Means With DIMNGF**	**0.9719**	**0.9463**
***k*-Means With DIMDGF**	**0.9758**	**0.9734**

Table 5: Correlation of tortuosity measures with expert's ground truth.

Tortuosity Measure	Correlation
L_{curve}/L_{chord} (Kalitzeos *et al.*; 2013)	0.73
TI_{freq1}	0.73
TI_{freq2}	0.80

DISCUSSION

This section presents a detailed discussion of the results obtained in this study.

COMPARISON WITH EXISTING SEGMENTATION METHODS ON DRIVE DATABASE

The *k*-means clustering techniques investigated achieved average sensitivity rates of 0.7079, 0.7399, 0.7518 and 0.7581 with corresponding average accuracy rates of 0.9523, 0.9556, 0.9531 and 0.9516 respectively on DRIVE database. All the techniques that combined difference image with *k*-means clustering presented significantly higher average sensitivity rates of 0.7079, 0.7399, 0.7518 and 0.7581 with significantly higher average accuracy rates of 0.9523, 0.9556, 0.9531 and 0.9516 when compared with the average sensitivity rates of 0.3357, 0.6389, 0.6399, 0.6971, 0.6562, 0.6565 and 0.6522 with their corresponding average accuracy rates of 0.8773, 0.9181, 0.9212, 0.9377, 0.9459, 0.9482 and 0.9267 achieved by Chaudhuri *et al.* (1989), Martínez-Pérez *et al.* (1999), Jiang and Mojon (2003), Zana and Klein (2001), Lupaşcu and Tegolo (2011a), Lupaşcu

and Tegolo (2011b) and Yin *et al.* (2013), respectively. All the techniques that combined difference image with *k*-means clustering presented significantly higher average average accuracy rates of 0.9523, 0.9556, 0.9531 and 0.9516 when compared with the average accuracy rate 0.9387 obtained by Saffarzadeh *et al.* (2014). Three of the techniques that combined difference image with *k*-means clustering presented significantly higher average sensitivity rates of 0.7399, 0.7518 and 0.7581 with significantly higher average accuracy rates of 0.9556, 0.9531 and 0.9516 when compared with the average sensitivity rates of 0.7145, 0.7345 and 0.7315 with their corresponding average accuracy rates of 0.9416, 0.9442 and 0.9463 presented by Niemeijer *et al.* (2004), Staal *et al.* (2004) and Mendonca and Campilho (2006) respectively.

Two of the techniques that combined difference image with *k*-means clustering presented significantly higher average sensitivity rates of 0.7518 and 0.7581 with significantly higher average accuracy rates of 0.9531 and 0.9516 when compared with the average sensitivity rate of 0.7468 and average accuracy rate of 0.9285 achieved by Vlachos and Dermatas (2010).

Although two of the techniques that combined difference image with *k*-means clustering presented higher average sensitivity rates of 0.7518 and 0.7581 when compared with Xiao *et al.* (2013) where an average sensitivity rate of 0.7513 was achieved, one of of the technique presented a significantly higher average sensitivity rate of 0.7581 when compared with the average sensitivity rate 0.7513 achieved by Xiao *et al.* (2013). All the *k*-means clustering techniques investigated achieved significantly higher average accuracy rates of 0.9523, 0.9556, 0.9531 and 0.9516 when compared with Soares *et al.* (2006), Szpak and Tapamo (2008), Marín *et al.* (2011), Akram and Khan (2013) and Wang *et al.* (2013) where no average sensitivity rate was presented but average accuracy rates of 0.9466, 0.9299, 0.9452, 0.9469 and 0.9461 were achieved respectively. All the difference images combined with *k*-means presented lower average sensitivity rates of 0.7079, 0.7399, 0.7518 and 0.7581 but significantly higher average accuracy rates of 0.9523, 0.9556, 0.9531 and 0.9516 when compared with the second human observer with average sensitivity rate of 0.7761 and average accuracy rate of 0.9473.

All the proposed *k*-means clustering techniques presented significantly higher AUC rates of 0.9719, 0.9735, 0.9749 and 0.9758 (see Table 4 and Figs. 13 and 14) when compared with the AUC rates 0.7878, 0.8984, 0.9114, 0.9294, 0.9520, 0.9614, 0.9558, 0.9588, 0.963, 0.9543 and 0.9303 achieved by the previously proposed techniques by Chaudhuri *et al.* (1989), Zana and Klein (2001), Jiang and Mojon

(2003), Niemeijer *et al.* (2004), Staal *et al.* (2004), Soares *et al.* (2006), Ricci and Perfetti (2007), Marín *et al.* (2011), Akram and Khan (2013), Wang *et al.* (2013) and Saffarzadeh *et al.* (2014) on DRIVE.

COMPARISON WITH EXISTING SEGMENTATION METHODS ON STARE DATABASE

The *k*-means clustering techniques investigated achieved average sensitivity rates of 0.6979, 0.7372, 0.7666 and 0.7772 with corresponding average accuracy rates of 0.9340, 0.9509, 0.9500 and 0.9492 respectively on STARE database. All the techniques that combined difference image with *k*-means clustering presented significantly higher average sensitivity rates of 0.6979, 0.7372, 0.7666 and 0.7772 with significantly higher average accuracy rates of 0.9340, 0.9509, 0.9500 and 0.9492 when compared with the average sensitivity rate of 0.6751 and average accuracy rate of 0.9275 achieved by Hoover *et al.* (2000). All the *k*-means clustering techniques investigated presented significant higher average accuracy rates of 0.9340, 0.9509, 0.9500 and 0.9492 when compared with the work of Jiang and Mojon (2003) that achieved an average accuracy rate of 0.9009.

Although all the techniques that combined difference image with *k*-means clustering presented higher average sensitivity rates of 0.6979, 0.7372, 0.7666 and 0.7772 when compared with the average sensitivity rate of 0.6951 achieved by Staal *et al.* (2004), only three of the average sensitivity have significant differences when compared with Staal *et al.* (2004). Three of the techniques that combined difference image with *k*-means clustering presented significantly higher average sensitivity rates of 0.7372, 0.7666, 0.7772 and significantly higher average accuracy rates of 0.9509, 0.9500 0.9492 when compared with the average sensitivity rates of 0.7123, 0.7147 and 0.7248 with corresponding average accuracy rates of 0.9479, 0.9476 and 0.9412 presented by Mendonca and Campilho (2006), Xiao *et al.* (2013) and Yin *et al.* (2013) respectively.

Ricci and Perfetti (2007), Marín *et al.* (2011) and Wang *et al.* (2013) presented no sensitivity but higher average accuracy rates 0.9584, 0.9526 and 0.9521 when compared with the average accuracy rates of all the *k*-means clustering segmentation techniques in the range 0.9340 to 0.9509. Akram and Khan (2013) presented no sensitivity but a lower average accuracy rate of 0.9502 when compared with average accuracy rate of 0.9509 obtained using one of the *k*-means clustering segmentation techniques with no significant difference. Soares *et al.* (2006) and Saffarzadeh *et al.* (2014) also presented lower

average accuracy rates of 0.9480 and 0.9483 when compared with the average accuracy rates of 0.9509, 0.9500 and 0.9492 obtained from three of the *k*-means clustering segmentation techniques with significant differences. The human observer STARE (2000) presented a higher average sensitivity of 0.88949 when compared with all the average sensitivity rates of *k*-means clustering segmentation techniques. The higher average sensitivity rate achieved by the human observer STARE (2000) showed the higher detection rate of both large and thin vessels by the human observer in the retinal images. The human observer STARE (2000), however, presented a significantly lower average accuracy rate of 0.9354 when compared with the average accuracy rates of 0.9509, 0.9500 and 0.9492 obtained from three of the *k*-means clustering segmentation techniques.

Three of the proposed *k*-means clustering techniques on STARE (see Table 4) presented significantly higher AUC rates of 0.9728, 0.9734 and 0.9756 when compared with the AUC rates of 0.929, 0.9614, 0.9671, 0.9602, 0.970, 0.9682 and 0.9431 achieved by Jiang and Mojon (2003), Staal *et al.* (2004), Soares *et al.* (2006), Ricci and Perfetti (2007), Akram and Khan (2013), Wang *et al.* (2013) and Saffarzadeh *et al.* (2014) respectively.

COMPARISON OF TORTUOSITY MEASURES WITH EXPERT'S GROUND TRUTH

The tortuosity measures computed in the previous section utilized chord length, arc length and the frequency of twists using the stationary points of the vessel curves.

The non-normalized tortuosity index (TI) combined a different distance metric and the vessel twist frequency as described in Eq. 11. The normalized TI as described in Eq. 10, utilized the chord length for the normalization previously presented distance metric combined with the twist frequency measure. A threshold value 1.0 is applied to differentiate tortuous from non-tortuous retinal vessels. Hence, TI values less than 1.0 are considered non-tortuous while TI values greater than or equal to 1.0 are considered to tortuous. Table 5 shows the correlation of the tortuosity measures obtained with the expert ground truth using Spearman's rank correlation coefficient. The result obtained shows that the non-normalised metric (TI_{freq2}) has a stronger correlation with the expert ground truth with significant differences when compared with the other techniques investigated.

In conclusion, this paper presents unsupervised vessel segmentation approach that combines difference image and *k*-means clustering for the segmentation of retinal vessels. *K*-means clustering combined with difference images addressed the major drawback of supervised segmentation methods which is their high dependence on the labelled training with the retraining of the classifiers. *K*-means clustering combined with difference image based on median filter also addressed the segmentation of large and thinner retinal vessels as well as the reduction of false detection around the border of the optic disc. It is also shown that an integration of difference images based on median filter with difference image based on mean filter and difference image based on Gaussian filter while combined with *k*-means clustering technique segmented both large and thin vessels in retinal images. The reason for the good performance of these segmentation techniques are due to the very good edge-preserving property of median filter. The vessel segmentation techniques that combined median filtered based difference image with *k*-means clustering technique present higher average sensitivity and average accuracy rates when compared with the previous techniques on DRIVE and STARE databases. The vessel segmentation techniques investigated in this paper are also computationally fast ranging from 3.4 to 4.0 seconds on DRIVE and STARE databases.

Having designed and implemented the detection of twists in vessel segments through the use of stationary points in the vessel center-lines, we also showed that the proposed non-normalized TI that combined the distance metric and the vessel twist frequency has a stronger correlation with the expert's ground truth when compared to the previously presented distance metric and the normalized TI investigated in this paper.

REFERENCES

Abràmoff MD, Garvin MK, Sonka M (2010a). Retinal imaging and image analysis. IEEE Rev Biomed Eng 3:169–208.

Abràmoff MD, Reinhardt JM, Russell SR, Folk JC, Mahajan VB, Niemeijer M, Quellec G (2010b). Automated early detection of diabetic retinopathy. Ophthalmology 117:1147–54.

Adio AO, Ugwu RO, Nwokocha CG, Eneh AU (2014). Retinopathy of prematurity in Port Harcourt, Nigeria. ISRN Ophthalmol 2014:481527.

Akram MU, Khan SA (2013). Multilayered thresholding-based blood vessel segmentation for screening of diabetic retinopathy. Eng Comput 29:165–73.

Atlas ID (2013). 6th edn. International Diabetes Federation Brussels Belgium :160.

Azegrouz H, Trucco E, Dhillon B, MacGillivray T, MacCormick I (2006). Thickness dependent tortuosity estimation for retinal blood vessels. In: Proc 28th IEEE Int Conf Eng Med Biol Soc (EMBS '06). Aug 30–Sep 3, 2006. 4675–8.

Bedell AJ (1945). Retinal vessel proliferation in diabetes. Trans Am Ophthalmol Soc 43:271.

Bribiesca E (2013). A measure of tortuosity based on chain coding. Pattern Recogn 46:716–24.

Bullitt E, Gerig G, Pizer SM, Lin W, Aylward SR (2003). Measuring tortuosity of the intracerebral vasculature from MRA images. IEEE T Med Imag 22:1163–71.

Capowski JJ, Kylstra JA, Freedman SF (1995). A numeric index based on spatial frequency for the tortuosity of retinal vessels and its application to plus disease in retinopathy of prematurity. Retina 15:490–500.

Chakraborti T, Jha DK, Chowdhury AS, Jiang X (2014). A self-adaptive matched filter for retinal blood vessel detection. Mach Vision Appl 26:55–68.

Chakravarty A, Sivaswamy J (2013). A novel approach for quantification of retinal vessel tortuosity using quadratic polynomial decomposition. In: Proc 2013 IEEE Indian Conf Med Inform Telemed (ICMIT) 7–12

Chanwimaluang T, Fan G (2003). An efficient blood vessel detection algorithm for retinal images using local entropy thresholding. In: Proc 2003 IEEE Int Int Symp Circuit Syst (ISCAS '03) 5:V21–4.

Chaudhuri S, Chatterjee S, Katz N, Nelson M, Goldbaum M (1989). Detection of blood vessels in retinal images using two-dimensional matched filters. IEEE T Med Imaging 8:263–9.

Chen Y, Li X, Yin H, Gilbert C, Liang J, Jiang Y, Zhao M (2008). Risk factors for retinopathy of prematurity in six neonatal intensive care units in Beijing, China. Br J Ophthalmol 92:326–30.

Cinsdikici MG, Aydın D (2009). Detection of blood vessels in ophthalmoscope images using MF/ant (matched filter/ant colony) algorithm. Comput Meth Prog Bio 96:85–95.

Condurache AP, Aach T (2006). Vessel segmentation in 2D-projection images using a supervised linear hysteresis classifier. In: Proc 18th IEEE Int Conf Pattern Recogn (ICPR '06) 1:343–6.

Cornforth D, Jelinek HJ, Leandro J, Soares J, Cesar Jr R, Cree MJ, Mitchell P, Bossomaier T (2005). Development of retinal blood vessel segmentation methodology using wavelet transforms for assessment of diabetic retinopathy. Complexity Int 11:50–61.

Davitt BV, Wallace DK (2009). Plus disease. Surv Ophthalmol 54:663–70.

Dougherty G, Johnson MJ, Wiers MD (2010). Measurement of retinal vascular tortuosity and its application to retinal pathologies. Med Biol Eng Comput 48:87–95.

Dougherty G, Varro J (2000). A quantitative index for the measurement of the tortuosity of blood vessels. Med Eng Phys 22:567–74.

DRIVE (2004). Research section, digital retinal image for vessel extraction (drive) database. Utrecht: utrecht, the netherlands, univ. med. center utrecht, image sci. inst. [available online]. http://www.isi.uu.nl/Research/Databases/DRIVE.

Foody GM (2009). Classification accuracy comparison: hypothesis tests and the use of confidence intervals in evaluations of difference, equivalence and non-inferiority. Remote Sens Environ 113:1658–63.

Fraz MM, Barman S, Remagnino P, Hoppe A, Basit A, Uyyanonvara B, Rudnicka AR, Owen CG (2012a). An approach to localize the retinal blood vessels using bit planes and centerline detection. Comput Meth Prog Bio 108:600–16.

Fraz MM, Remagnino P, Hoppe A, Uyyanonvara B, Owen CG, Rudnicka AR, Barman S (2011). Retinal vessel extraction using first-order derivative of Gaussian and morphological processing. In: Proc 7th Int Symp Visual Comput. Lect Not Comput Sci 6938:410–20.

Fraz MM, Remagnino P, Hoppe A, Uyyanonvara B, Rudnicka AR, Owen CG, Barman SA (2012b). Blood vessel segmentation methodologies in retinal images–a survey. Comput Meth Prog Bio 108:407–33.

Fraz MM, Remagnino P, Hoppe A, Uyyanonvara B, Rudnicka AR, Owen CG, Barman SA (2012c). An ensemble classification-based approach applied to retinal blood vessel segmentation. IEEE T Biomed Eng 59:2538–48.

Fraz MM, Rudnicka AR, Owen CG, Barman SA (2013). Delineation of blood vessels in pediatric retinal images using decision trees-based ensemble classification. Int J Comput Assist Radiol Surg 9:795–811.

Gergely K, Gerinec A (2009). Retinopathy of prematurity–epidemics, incidence, prevalence, blindness. Bratisl Lek Listy 111:514–7.

Grisan E, Foracchia M, Ruggeri A (2003). A novel method for the automatic evaluation of retinal vessel tortuosity. In: Proc 25th IEEE Int Conf Eng Med Bio Soc (EMBS '03) 1:866–9.

Grisan E, Foracchia M, Ruggeri A (2008). A novel method for the automatic grading of retinal vessel tortuosity. IEEE T Med Imag 27:310–9.

Grisan E, Pesce A, Giani A, Foracchia M, Ruggeri A (2004). A new tracking system for the robust extraction of retinal vessel structure. In: Proc 26th IEEE Int Conf Eng Med Bio Soc (EMBS '04) 1:1620–3.

Hakeem AH, Mohamed GB, Othman MF (2012).

Retinopathy of prematurity: a study of prevalence and risk factors. Middle East Afr J Ophthalmol 19:289–94.

Hart WE, Goldbaum M, Cote B, Kube P, Nelson MR (1997). Automated measurement of retinal vascular tortuosity. In: Proc AMIA Annu Fall Symp 459–63.

Hart WE, Goldbaum M, Côté B, Kube P, Nelson MR (1999). Measurement and classification of retinal vascular tortuosity. Int J Med Inform 53:239–52.

Heneghan C, Flynn J, OKeefe M, Cahill M (2002). Characterization of changes in blood vessel width and tortuosity in retinopathy of prematurity using image analysis. Med Image Anal 6:407–29.

Hoover A, Kouznetsova V, Goldbaum M (2000). Locating blood vessels in retinal images by piecewise threshold probing of a matched filter response. IEEE T Med Imaging 19:203–10.

Jiang X, Mojon D (2003). Adaptive local thresholding by verification-based multithreshold probing with application to vessel detection in retinal images. IEEE T Pattern Anal 25:131–7.

Jiménez S, Alemany P, Fondón I, Foncubierta A, Acha B, Serrano C (2010). Automatic detection of vessels in color fundus images. Arch Soc Esp Oftalmol 85:103–9.

Joshi GD, Sivaswamy J (2008). Colour retinal image enhancement based on domain knowledge. In: Proc 6th IEEE Ind Conf Comput Vision Graphics Image Proc (ICVGIP '08). 591–8.

Kalitzeos AA, Lip GY, Heitmar R (2013). Retinal vessel tortuosity measures and their applications. Exp Eye Res 106:40–6.

Kande GB, Subbaiah PV, Savithri TS (2010). Unsupervised fuzzy based vessel segmentation in pathological digital fundus images. J Med Syst 34:849–58.

Klonoff DC, Schwartz DM (2000). An economic analysis of interventions for diabetes. Diabetes Care 23:390–404.

Kristinsson JK, Gottfredsdóttir MS, Stefánsson E (1997). Retinal vessel dilatation and elongation precedes diabetic macular oedema. Br J Ophthalmol 81:274–8.

Kylstra J, Wierzbicki T, Wolbarsht M, Landers III M, Stefansson E (1986). The relationship between retinal vessel tortuosity, diameter, and transmural pressure. Graef Arch Clin Exp Ophthal 224:477–80.

Li B, Li HK (2013). Automated analysis of diabetic retinopathy images: Principles, recent developments, and emerging trends. Curr Diab Rep 13:453–9.

Li Q, You J, Zhang D (2012). Vessel segmentation and width estimation in retinal images using multiscale production of matched filter responses. Expert Syst Appl 39:7600–10.

Li Q, You J, Zhang D, Bhattacharya P (2006). A multiscale approach to retinal vessel segmentation using Gabor filters and scale multiplication. In: Proc 2006 IEEE Int Conf Syst Man Cyber (SMC '06) 4:3521–7.

Lim LS, Cheung CY, Lin X, Mitchell P, Wong TY, Saw SM (2010). Influence of refractive error and axial length on retinal vessel geometric characteristics. Invest Ophthalmol Vis Sci :iovs–10. 52:669–78.

Lisowska A, Annunziata R, Loh GK, Karl D, Trucco E (2014). An experimental assessment of five indices of retinal vessel tortuosity with the RET-TORT public dataset. In: Proc 36th IEEE Int Conf Eng Med Bio Soc 5414–7.

Lotmar W, Freiburghaus A, Bracher D (1979). Measurement of vessel tortuosity on fundus photographs. A Graef Arch Klin Exp Ophthal 211:49–57.

Lupaşcu CA, Tegolo D (2011a). Automatic unsupervised segmentation of retinal vessels using self-organizing maps and k-means clustering. In: Pizzo R, Lisboa PJG, eds. Computational Intelligence Methods for Bioinformatics and Biostatistics. Lect Not Comput Sci 6685:263–74.

Lupaşcu CA, Tegolo D (2011b). Stable automatic unsupervised segmentation of retinal vessels using self-organizing maps and a modified fuzzy c-means clustering. In: Fanelli AM, Pedrycz W, Petrosino A, eds. Fuzzy Logic and Applications. Lect Not Comput Sci 6857:244–52.

Lupascu CA, Tegolo D, Trucco E (2010). FABC: retinal vessel segmentation using AdaBoost. IEEE T Inf Technol Biomed 14:1267–74.

Mapayi T, Viriri S, Tapamo JR (2014). A new adaptive thresholding technique for retinal vessel segmentation based on local homogeneity information. In: Image and Signal Processing. Lect Not Comput Sci 8509:558–67.

Mapayi T, Viriri S, Tapamo JR (2015). Comparative study of retinal vessel segmentation based on global thresholding techniques. Comput Math Methods Med 2015:895267.

Marín D, Aquino A, Gegúndez-Arias ME, Bravo JM (2011). A new supervised method for blood vessel segmentation in retinal images by using gray-level and moment invariants-based features. IEEE T Med Imaging 30:146–58.

Martínez-Pérez ME, Hughes AD, Stanton AV, Thom SA, Bharath AA, Parker KH (1999). Retinal blood vessel segmentation by means of scale-space analysis and region growing. In: Taylor C, Colchester A, eds. Medical Image Computing and Computer-Assisted Intervention–MICCAI99. Lect Not Comput Sci 1679:90–7.

Martinez-Perez ME, Hughes AD, Stanton AV, Thom

SA, Chapman N, Bharath AA, Parker KH (2002). Retinal vascular tree morphology: a semi-automatic quantification. IEEE T Biomed Eng 49:912–7.

Mendonca AM, Campilho A (2006). Segmentation of retinal blood vessels by combining the detection of centerlines and morphological reconstruction. IEEE T Med Imaging 25:1200–13.

Miri MS, Mahloojifar A (2011). Retinal image analysis using curvelet transform and multistructure elements morphology by reconstruction. IEEE T Biomed Eng 58:1183–92.

Nekovei R, Sun Y (1995). Back-propagation network and its configuration for blood vessel detection in angiograms. IEEE T Neural Netw 6:64–72.

Niemeijer M, Staal J, van Ginneken B, Loog M, Abramoff MD (2004). Comparative study of retinal vessel segmentation methods on a new publicly available database. In: Proc SPIE 5370. Med Imaging 2004: Image Proc. 648.

Onkaew D, Turior R, Uyyanonvara B, Akinori N, Sinthanayothin C (2011). Automatic retinal vessel tortuosity measurement using curvature of improved chain code. In: Proc 2011 Int Conf Elec Contr Comput Eng (INECCE) 183–6.

Osareh A, Shadgar B (2009). Automatic blood vessel segmentation in color images of retina. Iran J Sci Technol Trans B 33:191–206.

O'Sullivan J, Gilbert C, Foster A (1997). The causes of childhood blindness in South Africa. S Afr Med J 87:1691–5.

Owen CG, Newsom RS, Rudnicka AR, Barman SA, Woodward EG, Ellis TJ (2008). Diabetes and the tortuosity of vessels of the bulbar conjunctiva. Ophthalmology 115:e27–e32.

Patasius M, Marozas V, Lukosevicius A, Jegelevicius D (2007). Model based investigation of retinal vessel tortuosity as a function of blood pressure: preliminary results. In: Proc 29th IEEE Int Conf Eng Med Biol Soc 6459–62.

Poletti E, Fiorin D, Grisan E, Ruggeri A (2011). Automatic vessel segmentation in wide-field retina images of infants with retinopathy of prematurity. In: Proc 2011 IEEE Annu Conf Eng Med Biol Soc 3954–7.

Poletti E, Grisan E (2014). Learning optimal matched filters for retinal vessel segmentation with ADA-Boost. In: Proc 13th Med Conf Med Biol Eng Comput. IFMBE Proc 41:380–3.

Poletti E, Ruggeri A (2012). Segmentation of vessels through supervised classification in wide-field retina images of infants with retinopathy of prematurity. In: Proc 25th IEEE Int Symp Comput Based Med Syst (CBMS) 1–6.

Prasanna P, Jain S, Bhagat N, Madabhushi A (2013). Decision support system for detection of diabetic retinopathy using smartphones. In: Proc 7th IEEE Int Conf Pervas Comput Technol Health 176–9.

Rechtman E, Harris A, Garzozi HJ, Ciulla TA (2007). Pharmacologic therapies for diabetic retinopathy and diabetic macular edema. Clin Ophthalmol 1:383–91.

Ricci E, Perfetti R (2007). Retinal blood vessel segmentation using line operators and support vector classification. IEEE T Med Imaging 26:1357–65.

Saffarzadeh VM, Osareh A, Shadgar B (2014). Vessel segmentation in retinal images using multi-scale line operator and *k*-means clustering. J Med Signals Sens 4:122.

Sasongko MB, Wang JJ, Donaghue KC, Cheung N, Benitez-Aguirre P, Jenkins A, Hsu W, Lee ML, Wong TY (2010). Alterations in retinal microvascular geometry in young type 1 diabetes. Diabetes Care 33:1331–6.

Scheie HG (1953). Evaluation of ophthalmoscopic changes of hypertension and arteriolar sclerosis. AMA Arch Ophthalmol 49:117–38.

Sinthanayothin C, Boyce JF, Cook HL, Williamson TH (1999). Automated localisation of the optic disc, fovea, and retinal blood vessels from digital colour fundus images. Br J Ophthalmol 83:902–10.

Sinthanayothin C, Panitsuk P, Uyyanonvara B (2010). Automatic retinal vessel tortuosity measurement. In: Proc 2010 Int Conf Elec Eng Electron Comput Telecomm Inf Tech (ECTI_CON) 505-7.

Soares JV, Leandro JJ, Cesar RM, Jelinek HF, Cree MJ (2006). Retinal vessel segmentation using the 2-D Gabor wavelet and supervised classification. IEEE T Med Imaging 25:1214–22.

Staal J, Abràmoff MD, Niemeijer M, Viergever MA, van Ginneken B (2004). Ridge-based vessel segmentation in color images of the retina. IEEE T Med Imaging 23:501–9.

STARE (2000). Stare (structured analysis of the retina) projectwebsite. Clemson, SC: Clemson Univ. [online], available: http://www.ces.clemson.edu/~ahoover/stare/.

Sun K, Chen Z, Jiang S, Wang Y (2011). Morphological multiscale enhancement, fuzzy filter and watershed for vascular tree extraction in angiogram. J Med Syst 35:811–24.

Sussman EJ, Tsiaras WG, Soper KA (1982). Diagnosis of diabetic eye disease. JAMA 247:3231–4.

Szpak ZL, Tapamo JR (2008). Automatic and interactive retinal vessel segmentation: pattern recognition special edition. South Afr Comput J 40:23–30.

Taarnhøj N, Munch I, Sander B, Kessel L, Hougaard J, Kyvik K, Sørensen TI, Larsen M (2008). Straight versus

tortuous retinal arteries in relation to blood pressure and genetics. Br J Ophthalmol 92:1055–60.

Thomas C (1996). Introduction to differential calculus. Sydney: University of Sydney.

Tolias YA, Panas SM (1998). A fuzzy vessel tracking algorithm for retinal images based on fuzzy clustering. IEEE T Med Imaging 17:263–73.

Varughese S, Gilbert C, Pieper C, Cook C (2008). Retinopathy of prematurity in South Africa: an assessment of needs, resources and requirements for screening programmes. Br J Ophthalmol 92:879–82.

Verma L, Prakash G, Tewari HK (2002). Diabetic retinopathy: time for action. No complacency please! B World Health Organ 80:419.

Vlachos M, Dermatas E (2010). Multi-scale retinal vessel segmentation using line tracking. Comput Med Imaging Graph 34:213–27.

Wang Y, Ji G, Lin P, Trucco E, et al. (2013). Retinal vessel segmentation using multiwavelet kernels and multiscale hierarchical decomposition. Pattern Recogn 46:2117–33.

Wasan B, Cerutti A, Ford S, Marsh R (1995). Vascular network changes in the retina with age and hypertension. J Hypertens 13:1724–8.

WHO (2010). Action plan for the prevention of avoidable blindness and visual impairment, 2009-2013. World Health Organization.

Wilson CM, Cocker KD, Moseley MJ, Paterson C, Clay ST, Schulenburg WE, Mills MD, Ells AL, Parker KH, Quinn GE, et al. (2008). Computerized analysis of retinal vessel width and tortuosity in premature infants. Invest Ophthalmol Vis Sci 49:3577–85.

Wolffsohn JS, Napper GA, Ho SM, Jaworski A, Pollard TL (2001). Improving the description of the retinal vasculature and patient history taking for monitoring systemic hypertension. Ophthalmic Physiol Opt 21:441–9.

Xiao Z, Adel M, Bourennane S (2013). Bayesian method with spatial constraint for retinal vessel segmentation. Comput Math Methods Med 2013:401413.

Yang Y, Huang S, Rao N (2008). An automatic hybrid method for retinal blood vessel extraction. Int J Appl Math Comput Sci 18:399–407.

Yin Y, Adel M, Bourennane S (2013). Automatic segmentation and measurement of vasculature in retinal fundus images using probabilistic formulation. Comput Math Methods Med 2013:260410.

You X, Peng Q, Yuan Y, Cheung Ym, Lei J (2011). Segmentation of retinal blood vessels using the radial projection and semi-supervised approach. Pattern Recogn 44:2314–24.

Zana F, Klein JC (2001). Segmentation of vessel-like patterns using mathematical morphology and curvature evaluation. IEEE T Image Process 10:1010–9.

Zhang B, Zhang L, Zhang L, Karray F (2010). Retinal vessel extraction by matched filter with first-order derivative of Gaussian. Comput Biol Med 40:438–45.